Journal of proteome research

Article

Proteomic alterations in response to Hypoxia Inducible Factor 2# in normoxic Neuroblastoma cells

Flora Cimmino, Lucia Pezone, Marianna Avitabile, Luca Persano, Monica Vitale, Mauro Sassi, Silvia Bresolin, Valentina Serafin, Nicola Zambrano, Andrea Scaloni, Giuseppe Basso, Achille Iolascon, and Mario Capasso

J. Proteome Res., **Just Accepted Manuscript** • DOI: 10.1021/acs.jproteome.6b00457 • Publication Date (Web): 05 Sep 2016

ACS Publications

Journal of Proteome Research is published by the American Chemical Society. 1155 Sixteenth Street N.W., Washington, DC 20036

Proteomic alterations in response to Hypoxia Inducible Factor 2α in normoxic Neuroblastoma cells

Flora Cimmino[1,2,*], Lucia Pezone[2-3], Marianna Avitabile[1,2], Luca Persano[4], Monica Vitale[1,2], Mauro Sassi[5], Silvia Bresolin[6], Valentina Serafin[6], Nicola Zambrano[1,2], Andrea Scaloni[5], Giuseppe Basso[6], Achille Iolascon[1,2], Mario Capasso[1,2]

[1] Dipartimento di Medicina Molecolare e Biotecnologie Mediche, Università degli Studi di Napoli "Federico II", Naples, Italy

[2] CEINGE Biotecnologie Avanzate, Naples, Italy

[3] Scuola di Medicina e Chirurgia, Università degli Studi di Verona, Verona, Italy

[4] Istituto di Ricerca Pediatrica Città della Speranza - IRP, Padua, Italy

[5] Proteomics and Mass Spectrometry Laboratory, ISPAAM, National Research Council, Naples, Italy

[6] Dipartimento di Salute della Donna e del Bambino, Università degli Studi di Padova, Padua, Italy

Keywords: Hypoxia inducible factor 2α, Neuroblastoma, Proteomics, Patient stratification

Corresponding Author:

Cimmino Flora, PhD

CEINGE – Biotecnologie Avanzate

Via Gaetano Salvatore 486

80145 Napoli, Italy

Email: cimminof@ceinge.unina.it

Phone: +39 081 3737 73

Summary

Hypoxia Inducible Factor (HIF)-2α protein expression in solid tumors promotes stem-like phenotype in cancer stem cells and increases tumorigenic potential in non-stem cancer cells. Recently, we have shown HIF-1/2α gene expression is correlated to neuroblastoma (NB) poor survival and to undifferentiated tumor state; HIF-2α protein was demonstrated to enhance aggressive features of the disease. In this study, we used proteomic experiments on NB cells to investigate HIF-2α downstream-regulated proteins and/or pathways with the aim of providing novel therapeutic targets and/or bad prognosis markers. We verified that pathways mostly altered by HIF-2α perturbation are involved in tumor progression. In particular, HIF-2α induces alteration of central metabolism and splicing control pathways. Simultaneously, WNT, RAS/MAPK and PI3K/AKT activity and/or expression are affected and may impact on the sensitivity and the intensity of HIF-2α-regulated pathways. Furthermore, genes coding the identified HIF-2α-related markers built a signature able to stratify NB patients with unfavorable outcome. Taken together, our findings underline the relevance of dissecting the downstream effects of a poor survival marker in developing targeted therapy and improving patient stratification. Future prospective studies are needed to translate the use of these data into the clinical practice.

Introduction

Hypoxia-inducible factors (HIF-1α, HIF-2α) are key mediators of the cellular response to low oxygen concentrations (hypoxia). In the absence of oxygen, they are stabilized against degradation and thereby coordinate hypoxia adaptation through the expression of several target genes involved in neo-angiogenesis, glucose transport and metabolism, which are required for tumor growth and metastasis formation [1]. HIF-1α participates in the initial response to hypoxia being most active during short periods (2–24 h) of intense hypoxia or anoxia (<0.1% O_2). Conversely, HIF-2α is active under mild hypoxia (<5% O_2) or normoxia [2,3]. Moreover, an hypoxia-independent regulation appears probable in the latter case, because there are examples of genes whose expression is regulated by HIF-2α in cells grown under normoxic conditions [4,5].

HIF-2α protein expression in tumor perivascular regions promotes stem-like phenotype in cancer stem cells and increases tumorigenic potential in non-stem cancer cells [6,7,8]. HIF-2α-driven molecular mechanisms in tumor development are different. For example, HIF-2α overexpression as well as the deletion of *EPAS1* (HIF-2α coding gene) increases the growth of KRAS-driven lung tumors in mice [9]. Particularly, aberrant HIF-2α levels rise up the expression of VEGFA and SNAIL, thus promoting angiogenesis and tumor invasion. By contrast, the complete loss of HIF-2α reduces the expression of the tumor suppressor *Scgb3a1*, a HIF-2α target gene [9]. Thus, the pharmacological inhibition of HIF proteins for cancer treatment, whether targeting HIF-1α and HIF-2α together or individually, may not be straightforward. Targeting the key actors of oncogenic transformation downstream to HIF-2α may be a fascinating way to improve the efficacy of tumor-focused therapies [10].

In order to establish the protein networks regulated by HIF-2α and to speculate which HIF-2α-related proteins may be therapeutic targets and/or poor prognosis markers, we have focused on neuroblastoma (NB), a childhood malignancy of the developing sympathetic nervous system. NB

patients present widespread hematogenous-based metastases in over 50% of cases [11]. Recently, introduced targeted therapies for NB patients include the small molecule inhibitor Crizotinib, which targets the receptor tyrosine kinase Anaplastic Lymphoma Kinase (ALK); this drug have shown good toleration results in a recent Phase 1 dose-escalation trial [12]. Moreover, monoclonal antibody targeting the disialoganglioside GD2 included in an immunotherapeutic regimen resulted in a dramatic increase in event-free survival from 46 to 66% [13]. However, despite these recent advances, most high-risk NB patients die as result of the disease [11]. HIF-2α knockout in NB samples impairs tumorigenesis and leads to a less aggressive/more differentiated phenotype [14]. Recently, we have shown HIF-1/2α gene expression is correlated to NB poor survival and to undifferentiated tumor state [5]. Interestingly, we demonstrated that HIF-2α overexpression enhances the aggressive features of NB cells by means of the expression of pro-invading and anti-adhesive CD55 antigen [15].

In this study, we aimed to unravel the molecular mechanisms that might support HIF-2α induced tumor progression by highlighting the proteomic changes induced by HIF-2α perturbation in NB cells. To this purpose, a combined 2D-DIGE/nanoLC-ESI-LIT-MS/MS approach and Reverse phase protein array (RPPA) were used. Moreover, we verified that the expression of genes coding the identified HIF-2α-related proteins generates a signature able to stratify NB patients in different risk sub-groups.

Experimental Procedures

Cell cultures

The human SHSY5Y-pcDNA and SHSY5Y-HIF-2α NB cell clones were generated as already described [15]. The cells were grown in DMEM medium supplemented with 10% heat-inactivated fetal bovine serum (FBS), 100 kU/L penicillin, and 100 mg/L streptomycin, at 37 °C, in 5% CO_2, in a humidified atmosphere.

Protein fractionation

Cellular pellets from SHSY5Y-pcDNA and SHSY5Y-HIF-2α NB clones were incubated in ice-cold lysis buffer (250 mM sucrose, 3 mM imidazole, pH 7.4, and 1 mM EDTA) in the presence of a protease inhibitor cocktail (Complete Mini EDTA-free, Roche), and were disrupted by 8-10 passes through a 22-guage needle. Then they were centrifuged at 16,000 x *g* for 20 min, at 4 °C. This procedure allowed us enriching the corresponding nuclear fractions; protein extraction was then performed as already described [16].

Cy-Dye labeling

After adjusting the pH value to 8.5, protein extracts (50 µg) from three biological replicates of SHSY5Y-pcDNA cells and three replicates of SHSY5Y-HIF-2α cells were labeled separately with 400 pmol of Cy3 and Cy5. A pool composed of equal amounts of all the samples (six in number) was prepared, labeled with Cy2 and used as a standard on all gels. Labeling reactions were performed on ice in the dark, for 30 min, and were quenched by addition of 1 mM lysine (final concentration). Samples were mixed and the final volume was adjusted to 450 µL with 7

M urea, 2 M tiourea, and 3% CHAPS. The samples were supplemented with 0.5% carrier ampholytes pH 3-11 (GE Healthcare, Milan, Italy) and 1% bromophenol blue.

2-D Gel Electrophoresis and DIGE Analysis

For 2D-DIGE, IPG strips (length, 24 cm; thickness, 0.5 mm) (GE Healthcare) non-linear pH gradient range 3-11 were passively rehydrated with 150 μg of tripartite-labeled sample (50 μg for each labeled sample and 50 μg internal standard), in the dark, overnight. IEF was performed using an IPGphor II apparatus (GE Healthcare) at 20 °C, with a maximum current setting of 50 μA/strip, in the dark. IEF run conditions were the following: linear voltage up to 200 V in 1 h, up to 1000 V in 1 h, up to 1500 V in 1 h, up to 3500 V in 1 h, constant voltage to 3500 V for 3 h, linear voltage up to 5000 V in 1 h, constant voltage to 5000 V for 4 h, linear voltage up to 8000 V for 1 h, and constant voltage to 8000 V, until the total product time × voltage applied was 76,000 Vh for each strip. The strips were equilibrated in 6 M urea, 2% SDS, 20% glycerol, and 0.375 M Tris–HCl (pH 8.8), for 15 min, in the dark, in the presence of 0.5% w:v DTT, and then in the presence of 4.5% w/v iodacetamide in the same buffer, for additional 15 min. Equilibrated IPG strips were transferred onto 11% polyacrylamide gels, within low-fluorescence glass plates (ETTAN-DALT 6 system, GE Healthcare). Second-dimension SDS-PAGE was performed by using a DALT II electrophoresis unit (GE Healthcare) at 2 W/gel for 12 h. Gels were scanned with a Typhoon 9400 variable mode imager (GE Healthcare), using appropriate excitation/emission wavelengths for Cy2 (488/520 nm), Cy3 (532/580 nm), and Cy5 (633/670 nm). Images were acquired in the Image-Quant software (GE Healthcare) and analyzed by using the DeCyder 6.0 software (GE Healthcare) [16]. A DeCyder differential *in-gel* analysis (DIA) module was used for spot detection and pair-wise comparison of each sample (Cy3 and Cy5) to the Cy2 standard present in each gel. The DeCyder biological variation analysis (BVA) module

was used to simultaneously match all the proteomic maps from the gels, and to calculate average abundance ratios and *P* values across the triplicate sets of samples (Student's t-test).

For preparative gel electrophoresis, 1 mg of unlabeled sample was used to passively rehydrate the IPG strips. The first and second dimension runs were conducted as described above. After 2-D electrophoresis, the separated proteins were visualized using a highly sensitive fluorescent stain (SYPRO Ruby Protein Gel Stain, Life Technologies). Briefly, the resolved polypeptides were fixed in 7% acetic acid/50% methanol solution for 30 min, and stained overnight. The gels were washed in 7%acetic acid/10% methanol for 30 min, and in H_2O for 30 min. Finally, gels were scanned as mentioned above.

Mass spectrometry analysis and protein identification

Protein spots were excised from the preparative gel, alkylated, digested with trypsin and identified as previously reported [17]. Peptide mixtures were desalted by μZip-TipC18 (Millipore, USA) using 50% v/v acetonitrile/5% v/v formic acid as eluent before nanoLC-ESI-LIT-MS/MS analysis. Tryptic digests were analyzed using a LTQ XL mass spectrometer (Thermo, USA) equipped with a Proxeon nanospray source connected to an Easy nanoLC (Thermo, USA). Peptide mixtures were separated on an Easy C_{18} column (10 – 0.075 mm, 3 μm) (Thermo, USA) [18]. Mobile phases were 0.1% v/v aqueous formic acid (solvent A) and 0.1% v/v formic acid in acetonitrile (solvent B), running at total flow rate of 300 nL/min. Linear gradient was initiated 20 min after sample loading; solvent B ramped from 5% to 35% over 15 min, from 35% to 95% over 2 min. Spectra were acquired in the range *m/z* 400–1800. Acquisition was controlled by a data-dependent product ion scanning procedure over the 3 most abundant ions, enabling dynamic exclusion (repeat count 1 and exclusion duration 60 s); mass isolation window and collision energy were set to *m/z* 3 and 35%, respectively. MASCOT search engine version 2.2.06 (Matrix

Science, UK) was used to identify protein spots from a non-redundant human database (NCBI downloaded June 2014), using nanoLC-ESI-LIT-MS/MS data. Database searching was performed selecting trypsin as proteolytic enzyme, a missed cleavages maximum value of 2, Cys carbamidomethylation and Met oxidation as fixed and variable modification, respectively. Candidates with at least 2 assigned peptides with an individual MASCOT score >25, both corresponding to *p*-value <0.05 for a significant identification, were further evaluated by the comparison with their calculated mass and p*I* values, using the experimental data obtained from 2D-DIGE.

Data Mining

Differentially represented proteins between HIF-2α-overexpressing (HIF-2α) and control cells (pcDNA) were classified using the DAVID 2.1 beta annotation system (http://david.niaid.nih.gov/david/ease.htm). This tool adopts the Fisher exact test to measure the gene enrichment in annotation terms. A *p*-value <0.05 was considered statistically significant. We performed a gene enrichment analysis that included biological process and Kegg pathways terms.

Oil red staining

Eighty thousand cells were seeded on treated glass slide (BD Falcon, REF 354108). The day after the cells were fixed in 10% formalin for 10 min, and then rinsed 3 times in PBS. Slides were then placed in Oil Red O (Lipid Stain) solution for 10 min, rinsed in tap water, and counterstained with hematoxylin for 1 min (Abcam). Sections were then mounted in

Fluoromount-G and coverglassed. The images were acquired using a DMI4000B microscope (Leica Mycrosystem).

Western Blotting

For DIGE data validation, equal amount of nuclear extracts (25 μg) were loaded onto 8% or 12% polyacrilamide gels and transferred to PVDF membrane (Biorad) as described [16]. Membranes were incubated under constant shaking with the primary antibodies reported in Table S1, overnight, at 4 °C. H3 was used as loading control. For phosphoproteomics data validation, total protein extracts were isolated in lysis buffer as previously described [19]. Membranes were incubated under constant shaking with primary antibodies reported in Table S1, overnight, at 4 °C. β-Actin (Sigma Aldrich) was used as loading control. Membranes were next incubated with peroxidase (HRP)-conjugated anti-rat, anti-mouse, anti-rabbit and anti-goat antibodies (GE Healthcare). All the bands were visualized using ECL kit SuperSignal West Pico Chemiluminescent Substrate (Pierce), were acquired with a GelDoc 2000 system (Bio-Rad) and quantified by densitometry measurements using the Quantity One 4.5 tool (Bio-Rad).

Reverse Phase Protein Array (RPPA)

Reverse phase protein array analysis was performed as previously described with few adjustments [20]. Briefly, protein lysates were printed in 3-point dilution curves in quadruplicate on nitrocellulose-coated glass slides (ONCYTE® Nitrocellulose Film Slides, Grace BioLabs) with the 2470 Arrayer (Aushon BioSystems). Slides were stained for total protein content (Fast Green FCF; Sigma-Aldrich) and with 79 validated primary antibodies (Table S2) on an automated slide stainer (Dako Autostainer Plus, Dako-Cytomation). Signal amplification stage was performed

through the incubation with streptavidin-biotin-HRP complexes, VECTASTAIN Elite ABC Kit (VECTOR) 20 μL/mL in PBS 0.1% BSA for 15 min, followed by the incubation with the tyramide-biotin complex (TSA Plus Biotin Kit, PerkinElmer) at the dilution of 1:75 in Amplified Buffer for 10 min, and finally with HRP-Streptavidin (Dako-Cytomation) diluted 1:250 for 20 min. Signal was revealed using diaminobenzadine/hydrogen peroxide (DAB) as a chromogen substrate for 5 min (Dako-Cytomation). TIF images of antibody- and Fast Green FCF-stained slides were analyzed using the Microvigene software (VigeneTech Inc) to extract numeric intensity protein values from the array images.

Production of lentiviral particles and infection of cell lines

To knock-down *EPAS1* expression, the pGIPZ lentiviral shRNAmir that targets human *EPAS1* was purchased from Open Biosystems (Thermo Fisher Scientific, Inc.). We used two different shRNAs against *EPAS1*: V2LHS113750 (RHS4430-98894439) and V2LHS-113750 (RHS4430-98851126). A non-silencing pGIPZ lentiviral shRNAmir was used as the control (RHS4346). Lentiviral particles production and *in-vitro* transduction was performed as described [5].

Experimental design and Statistical evaluation

We have analyzed the proteins differentially represented between SHSY5Y cells transfected with empty vector pcDNA and SHSY5Y cells stable overexpressing HIF-2α protein. We have used three different replicates for each experimental point for DIGE analysis; DIGE data were subjected to the ANOVA test. For phosphoproteomic analysis, we assayed two different HIF-2α and pcDNA clones for each experimental point. Moreover, we used the cells silenced for the HIF-2α coding gene (*EPAS1*) given the sensitivity of pathways balance activation/inhibition in

the cells. Statistical analyses were performed with R (www.r-project.org). In particular, identification of potential differences in protein expression was obtained by using the Welch *t*-test and considered significant when *p*-value <0.05. Comparison between HIF-2α overexpressing cell clones and relative control cells was performed by considering the whole expression profile of specific pathways and *p*-values generated using global test applying 5000 permutations [19]. Hierarchical clustering analysis was performed using Eucledian distance among protein expression and Ward method clustering. Finally, levelplot form lattice package (R Biocoductor) was used to highlight the levels of relative protein expression between HIF-2α-silenced and -overexpressing cells, according to selected pathways.

HIF-2α proteome signature

K-mean clustering was performed using default parameters by methods implemented in program R2 (http://r2.amc.nl). The probability of overall survival (OS) and event free survival (EFS) was calculated using the Kaplan-Meier method, and the significance of the difference between Kaplan-Meier curves was calculated by the log-rank test (http://r2.amc.nl). The Cox regression model was used to test for the independent predictive ability of the HIF-2α proteome signature after the adjustment for other significant factors: MYCN amplification, age, INSS stages.

Results

2D-DIGE highlights differentially represented proteins as result of HIF-2α over-expression in SHSY5Y NB cells

SHSY5Y-HIF-2α overexpressing cells and SHSY5Y-pcDNA cells were obtained as previously reported [15]. HIF-2α induction on protein and mRNA levels in SHSY5Y cells are shown in Figure S1. The functional characterization of these clones showed that HIF-2α overexpression enhances the aggressive features of NB cells. Here we explored the molecular mechanisms that might generate the aggressive behavior mediated by HIF-2α. To this purpose, the cellular proteome was divided in two different cellular fractions, enriched either in cytosolic or nuclear proteins [16]. We checked the quality of these fractions by western blotting using specific markers, namely the nuclear protein lamin β (LMβ) and the cytosolic protein GAPDH. In fact, LMβ is mostly detected in the nuclear fraction, whereas GAPDH generally occurs in the cytosolic counterpart and, at lower levels, in the nucleus. We verified that this nuclear fraction also contained mitochondrial, lysosomal and Golgi subcellular compartments, as evidenced by positive staining for the corresponding marker cytochrome P450 reductase, lysosome-associated membrane glycoprotein 2 (LAMP2) and Golgi reassembly stacking protein of 55 kDa (GRASP55), respectively (Figure 1A). The nuclear fraction from SHSY5Y-HIF-2α and SHSY5Y-pcDNA cells was then considered for further experiments.

Proteomic changes associated with HIF-2α over-expression were analyzed using 2D-DIGE. To increase biological and statistical significance of the results, we prepared protein extracts from three independent SHSY5Y-HIF-2α and SHSY5Y-pcDNA cell cultures; they were labeled with either Cy3 or Cy5 fluorescent dyes according to the scheme shown in Table S3. Each Cy3/Cy5-labeled sample pair was co-mixed with a Cy2-labeled pooled standard sample containing an equal amount of the six samples; Cy2/Cy3/Cy5-labeled samples run together on the same gel.

For each gel, the Cy3, Cy5, and Cy2 images were imported into the DeCyder DIA module and analyzed with the BVA module of DeCyder software to reveal constant and differentially represented protein spots (see experimental section for details). Approximately, 1390 protein spots were detected in the SHSY5Y proteomic maps. They were then filtered for fold changes >1.3 or <1.3 (HIF-2α *vs* pcDNA) and p-*value*<0.05 (Student's paired *t* test) The analysis allowed us to find 53 statistically relevant and differentially represented spots, whose position on the gel is shown in Figure 1B. In particular, 21 spots were over-represented and 32 spots were under-represented. The same software modules were also used to match the Cy2 image selected as the master image with the counterpart from a preparative gel obtained by combining all cellular extracts. Corresponding spots from the latter gel were excised, *in-gel* digested with trypsin and subjected to nanoLC-ESI-LIT-MS/MS analysis for protein identification. Mass spectrometric analysis identified 49 proteins in 44 spots (Table 1). In several cases, different proteins co-migrated in the same spot; in other cases, the same protein occurred in different spots as result of eventual post-translational modifications. In this study, we were not able to determine the identities of the protein components of other 9 differentially represented spots. Identified proteins were then classified according to indicated descriptors for biological processes and molecular pathways; most of them were associated with cellular metabolism, RNA processing/splicing control and cell death (Figure 1C). The hypothesis that aggressive tumors have an abnormal cellular metabolism was also supported by gene ontology analysis on NB gene expression microarray datasets. As shown in supplementary data (Figure S2) "primary metabolic process" and "macromolecule metabolic process" were the more represented biological processes in relapse patient group.

Validation of differentially represented proteins and metabolic implications

We validated the differential (SHSY5Y-HIF-2α *vs* -pcDNA) representation pattern of a dozen of the proteins highlighted by 2D-DIGE analysis by western blotting (Figure 2A, Table S1). Densitometric analysis of protein bands demonstrated proteins representation as result of HIF-2α overexpression in NB cells (Figure 2B). In particular, we verified that DLAT, a component of the pyruvate dehydrogenase (PDH) complex, is over-represented as result of HIF-2α overexpression. To further assess PDH complex regulation, we also investigated the representation of pyruvate dehydrogenase (lipoamide) β (PDHB) subunit in SHSY5Y-HIF-2α and SHSY5Y-pcDNA cells by western blotting. These results highlight that HIF-2α over-expression induces metabolic changes in NB cells that lead to an increment of pyruvate and acetyl-CoA; this condition may ultimately conduce to cellular fatty acid storage. Accumulation of fatty acids in HIF-2α overexpressing cells was also supported by the down-representation of the fatty acid β-oxidation enzyme ECHS1 (2D-DIGE data – spot 1289). This metabolic condition was finally assessed by comparative oil red staining of SHSY5Y-HIF-2α and -pcDNA cells, which demonstrated an increase of fat droplets in NB cells as result of HIF-2α over-expression (Figure 2C-D).

The differential representation patterns of these HIF-2α targets were validated in NB cells silenced for HIF-2α expression. Particularly SHSY5Y and SKNBE2c cells were infected with lentiviral particles to silence the expression of *EPAS1* (Figure S1). As shown in supplementary data (Figure S3) the expression of HIF-2α targets are not strongly modified or are unvaried upon *EPAS1* silencing (shEPAS1 *vs* -shCTR). However protein expressions in silenced cells (shEPAS1 *vs* shCTR) are inverse respect to expression observed in HIF-2α overexpressing cells (HIF-2α *vs* pcDNA). These findings suggest that the identified targets are regulated by down-stream effects of HIF-2α overexpression. The down regulation of GSTP1 is convergent in HIF-2α overexpressing clones and in *EPAS1* silenced cells. GSTP1 is a detoxification enzyme which play an important role in neoplastic cells. On the other hand GSTP1 silencing is a common early

event in carcinogenesis, frequently caused by promoter hypermethylation [21]. Our finding suggest HIF-2α peculiarity to act differently in the same cells in response to diverse stimuli.

RPPA analysis of signalling pathways activated following HIF-2α over-expression in SHSY5Y NB cells

To account for the potential modulation of signalling pathways exerted by HIF-2α, we performed RPPA analysis of whole cell lysates to evaluate the expression of specific proteins (79 in number) (Table S2), among which 56 ones are activated/inhibited after phosphorylation at specific residues. For this reason, we compared the phosphorylation events activated/inhibited by HIF-2α overexpression with the counterpart induced by HIF-2α silencing. To avoid false positive/negative results, we performed RPPA analysis of SKNBE2c and SHSY5Y NB cells stably knocked-down for *EPAS1* transcript or SHSY5Y NB cells engineered to over-express HIF-2α. We observed an increased susceptibility to HIF-2α phosphoproteomic modifications in perturbated cells (HIF-2α overexpressing or *EPAS1* silenced cells) rather than alterations of quantitative levels of protein targets.

RPPA data were analyzed and then expression values of each protein were calculated. Protein expression values of HIF-2α silenced/over-expressing cells were compared to that of the appropriate control cells (shCTR/pcDNA). Statistical analysis was performed for all comparisons and obtained *p*-values were arrayed to generate a level-plot showing the potential differential activation of signalling pathways considered. In particular, analyzed proteins were divided for their relation with cellular pathways in order to cover JAK/STAT, NFKB, RAS/MAPK, SRC, WNT, AMPK, PI3K/AKT signalling pathways, apoptosis and cell cycle processes (Figure 3A). Since we did not observe any particular recurrence of single differentially represented (phospho) proteins between HIF-2α-silenced/-overexpressing cells and their relative controls, apart for

ERK1/2 and AKT phosphorylation, we re-analyzed data by performing a pathway global test, taking into account the overall expression of all the proteins belonging to a determined signalling pathway. As a result, RAS/MAPK, Wnt and PI3K/AKT pathways showed a significant (*p* value <0.05) under-activation upon HIF-2α silencing in at least one comparison (Figure 3B); conversely, RAS/MAPK, Wnt, PI3K/AKT, with the addition of cell cycle pathways were all over-activated in at least one HIF-2α-over-expressing cell clone (Figure 3B). Of note, although not all global tests resulted to be significant in every comparison we performed, relative expression of proteins (graphed as level plot in Figure 3C) showed a clear modulation of selected pathways in HIF-2α-silenced and -overexpressing cells. Importantly, hierarchical unsupervised analysis showed that the expression value of proteins belonging to the selected pathways were sufficient to completely identify HIF-2α-silenced and over-expressing cells (Figure 3D), thus underlining the potential involvement of RAS/MAPK, cell cycle, Wnt and PI3K/AKT pathways as downstream effectors of HIF-2α activation. Recently HIF-2α has been shown as a target of mTORC2 [22]. We verified that upon mTOR inhibition in SHSY5Y pcDNA and HIF-2α clones endogenous HIF-2α mRNA levels decreased but ectopic HIF-2α mRNA expression did not. This suggest HIF-2α is a direct transcriptional target of mTORC in SHSY5Y and HIF-2α overexpression might activate PI3K-pathway by promoting an autocrine loop (Figure S4).

The identified differentially activated pathways may be considered as the key regulators of fundamental cancer cell features, such as survival, differentiation, proliferation and cell metabolism, providing a rationale to the above-described differential representation of proteins, as identified by 2D-DIGE analysis.

Interestingly, phosho-FAK, which is involved in cell migration and motility, resulted over-activated in HIF-2α over-expressing cells (Figure 3A), suggesting its potential involvement in sustaining HIF-2α-mediated pro-cancerous effects, as reported above.

In order to validate our RPPA data, we performed Western blot analysis for RB (S780), cyclin-E, PAN-RAS, Erk1/2 (T202/Y204), LEF1, AKT (S473), S6 Ribosomal protein and PDK1 (S241) on HIF-2α-silenced/-over-expressing SHSY5Y cells (Figure 3E), confirming previous results on their inhibition/activation (Figure 3A).

Prognostic value of the HIF-2α proteomic signature

We speculated that the gene set codifying for the proteins differentially represented as result of HIF-2α expression may form a signature reflecting the aggressive features in NB (Table S4). The proteome-signature proposed for the stratification of NB patients with unfavorable outcome consists of the genes listed in Table 1.

As a first analysis of this signature, we investigated the prognostic value of the HIF-2α proteome- gene set. To this purpose, we used K-means clustering to subdivide the freely available gene expression data of 498 primary NB tumors at all stages (accession no. GSE62564) in two groups, having high or low activity of the HIF-2α proteome-gene set signature (Figure 4). One cluster of 157 tumors included the most of high-risk samples (Table S4) and showed high expression of up-regulated genes and low expression of down-regulated genes; accordingly, it was named HIF-2α proteome-POS. Another cluster of 341 NB tumors included most of the low-risk samples (Table 4S), having low expression of up-regulated genes and high expression of down-regulated genes; it was designated as HIF-2α proteome-NEG. Kaplan-Meier analysis of the two clusters showed that tumors with a HIF-2α proteome-POS signature conferred an extremely poor prognosis (log-rank test OS p $=3.7\text{x}10^{-33}$, EFS p= $3.9\text{x}10^{-24}$) (Figure 4A). Amplification of MYCN is an established marker for NB poor prognosis [11] (Figure 2S). HIF-2α proteome-POS signature conferred a poor prognosis independently from MYCN amplification, as observed in patients with MYCN single copy (OS p = 2.1×10^{-17}, EFS p= $7.9\text{x}10^{-16}$) (Figure

4B). Furthermore to test whether the HIF-2α proteoma signature is an independent prognostic factor in the NB samples, we performed multivariate Cox regression analysis of available prognostic factors, including the HIF-2α proteoma signature, age at diagnosis, INSS stage and MYCN status. The HIF-2α proteome signature turned out to be the most significant prognostic marker in addition to age, INSS stage the MYCN status (Table S5).

Discussion

NB is a heterogeneous and complex tumor whose development has not been completely elucidated. Several clinical studies demonstrated that HIF-2α correlates with NB advanced clinical stage and poor prognosis. We have recently reported that HIF-2α mRNA expression is correlated to metastatic NB potential and HIF-2α protein expression enhances pro-invading ability in NB cells [5,15].

HIF-2α response to various stimuli is different in organs and cancers [9]. In this study, we have distinguished specific markers/pathways activated by HIF-2α in NB progression. We verified that cellular metabolism, RNA processing/splicing control and cell death represent the most relevant biological processes in support of aggressive tumor phenotype and might result important for a successfully therapy. A shift in global splicing regulation has been previously reported in high-risk NB tumors [23]. In the cellular system under investigation, we observed: i) an over-representation of the heterogeneous nuclear ribonucleoprotein (hnRNP)K, which is known to promote metastasis *in vitro* and *in vivo* [24]; ii) a down-representation of hnRNPM, whose restricted activity promotes breast cancer metastasis via alternative splicing [25]; iii) an over-representation of hnRNPU, which can modulate WT1 transcription activation in Wilm's tumors [26]; iv) an over-representation of heat shock proteins HSPA8 and HSPA1A, which have been verified as poor prognosis signals in some other cancers for the regulation and stability of onco-transcription factors [27]. Coordinating splicing factors may have role or might act in opposite manners in other cancers. Understanding how HIF-2α may induce NB splicesome shift contributes to more aggressive phenotype can lead to the development of new class of anticancer therapeutics-alternative splicing inhibitors.

The altered metabolism has been established one of the hallmark of cancer over last decades [28]. We further confirmed the association of the carbon metabolism to malignancy by observing the correlation of metabolic processes to NB relapse in two patient cohorts. In HIF-2α-over-

expressing cells, we observed an increased representation of pyruvate dehydrogenase complex (PDH), which catalyzes the conversion of pyruvate to acetyl-coenzyme A (acetyl-CoA). In addition, we verified augmented levels of dihydrolipoamide S-acetyltransferase (DLAT), a component of the PDH complex, which was previously observed regulating cellular metabolism and mitochondrial functions [29]. Acetyl-CoA resources may be also provided by inhibition of fatty acid oxidation consequently to decrement of enoyl CoA hydratase (ECHS1). Thus, we might hypothesize that HIF-2α, and not hypoxia, drives NB cells onco-progression through the block of tricarboxylic acid cycle (TCA) and the increment of fatty acids synthesis. Acetyl-CoA may also impose an increment of acetate, which regulates the interaction of HIF-2α with its selective coactivator to the promoter of HIF-2α target genes or tumor progression genes [30]. Furthermore, a pseudohypoxic response that is conveyed by HIF-s is observed. In effect the increment of succinate dehydrogenase (SDH) and succinate CoA ligase (SUCLG2) may be responsible for the increment of succinate or fumarate, whose accumulation in mitochondria inhibits a family of prolyl hydroxylase enzymes (PHDs) [31]. In addition the suppressed expression of LDHB (Lactate Dehydrogenase B) may lead to lactate accumulation and oxidative metabolism increment as observed in pancreatic cancers [32].

There are some approved drugs directed toward cancer metabolism targets. For instance, glycolytic inhibitors, such as GLUT1 inhibitor and 2-deoxyglucose, underwent clinical trials [33]. Most cancer cell type are addicted to fatty acids, which they require for membrane phospholipid synthesis, signaling purpose and energy production. The deployment of potentially inhibitors to target clinically this facet of tumor metabolism is still under consideration [34]. We suggest that the administration of metabolic inhibitors in HIF-2α positive tumors foster an unsupportable conflation of growth promotion and substrate deficiency, with subsequent metabolic catastrophe. Intensive research in recent years has endeavored to determine how the metabolic activity of tumors is regulated. Distinguishing intracellular pathways in support to metabolic activity might

suggest the use of a combination therapy with the final aim to avoid resistance to metabolic block. PI3K/AKT pathway alteration following HIFs is a known regulator of cancer metabolism and cancer progression [35]. Recently, WNT signaling pathway has emerged as a regulatory mediator of cancer cells metabolic activities [36]. Additionally, RAS signaling activation is able to enhance glycolysis, TCA cycle and *de novo* nucleic acid synthesis by reprogramming the glycolytic and mitochondrial metabolism through the redox balance of NADH [37]. Of note, RAS-MAPK pathway is essential for HIF-2α transactivation and genes pathway mutations may occur in relapsed NB [38,39]. The increased activity and/or expression of WNT, RAS/MAPK and PI3K/AKT in our cellular system suggest that these pathways may fine-tune the sensitivity and the intensity of HIF-2α driving metabolism. Moreover, recent evidences report that RAS/MAPK and PI3K/AKT pathways converge to the regulation of mRNAs nucleocytoplasmic export [40,41]. Nonetheless, the crosstalk (in both directions) between cellular metabolism and mRNAs processing has still to be depicted and targeting in parallel metabolism and/or RNA splicing pathways is challenging.

Gene signatures identified to predict NB prognosis have shown a limited clinical value. Here we verified that the gene set codifying the proteins differentially represented by HIF-2α over-expression forms a signature reflecting the aggressive features in NB and having a high power of prognosis prediction. Particularly, this signature is able to identify the patients with negative outcome, which would benefit from new and more aggressive treatments. Future prospective studies are needed to further consolidate the validity of these data.

Conclusions

In the present study, we have dissected which proteins and pathways are regulated by HIF-2α in support to the aggressive features acquired by NB cells, when this transcription factor is over-

expressed. We have speculated that HIF-2α perturbation leads to an increment of fatty acid storage, which may maintain proliferation and energy production in cancer cells. Clinically targeting this facet of tumor metabolism may inhibit the mechanism for tumor cells to satisfy their strict metabolic requirement. However, the partial inhibition of a pathway may induce the tumor to find the way to evade the metabolic block. For this reason, we investigated the intracellular mediators that may regulate the metabolic activity by means of fine-tuning the sensitivity and intensity of HIF-2α pathways. The inhibition of deregulated intracellular mediators, such as RAS/MAPK, PI3K/AKT and WNT, may be relevant for developing more accurate and focused therapy, in combination with anti-metabolic drugs or splicing inhibitors. An interesting novelty of the presented approach has been to identify a gene signature able to stratify NB patients in two risk-subgroups starting from proteomic analysis. These findings provide the most reliability of a proteomic screening compared to gene expression screening. In conclusion, the presented approach has provided additional markers/pathways to be considered in developing targeted therapy and improving prognosis as alternative to HIF-2α in solid tumors. The feasibility to test this proteomic approach to un-drugable markers should finally result in the type of progress to avoid undesirable side-effects.

Supporting Information.

The following files are available free of charge on the ACS Publications website http://pubs.acs.org: Figure S1, HIF-2α protein and mRNA levels in HIF-2α overexpressing clones and *EPAS1* silenced clones; Figure S2, Gene Ontology analysis in two cohorts of NB relapsed patients; Figure S3, HIF-2α target proteins expression in *EPAS1* silenced cells; Figure S4, HIF-2α is a direct transcriptional target of mTORC in SHSY5Y cells and Figure S5, Prognostic value of the HIF-2α proteomic signature. Table S1, Antibodies used for Western Blotting; Table S2, Antibodies used for Reverse Phase Protein Array; Table S3, Experimental design of 2D-DIGE; Table S4, Tumor characteristics of two NB gene clusters and Table S5, Multivariate Cox regression Analyses.

Conflicts of interest

The authors declare that they have no conflicts of interest.

Acknowledgements

This study was supported by the Associazione Italiana per la Ricerca sul Cancro (AIRC) (11869) (AI); "Fondazione Italiana per la Lotta al Neuroblastoma" (MC); OPEN Associazione Oncologica Pediatrica e Neuroblastoma (AI, MC); Fondazione Istituto di Ricerca Pediatrica Città della Speranza and Fondazione CARIPARO (IRP13/05) (GB); Associazione Culturale *DiSciMuS* RFC (Progetto Biologia dei Tumori Ipossici) (NZ). FC was supported by a Fondazione Umberto Veronesi post-Doc Fellowship. VS was supported by a post-doctoral fellowship by AIRC. Authors are grateful to Dr. Benedetta Accordi from University of Padova for technical help in RPPA setup.

References

1) Lu, X.; Kang, Y.; Hypoxia and hypoxia-inducible factors: master regulators of metastasis. *Clin Cancer Res.* 2010, 16, 5928-35.

2) Zhao, J.; Du, F.; Luo, Y.; Shen, G.; Zheng, F.; Xu, B. The emerging role of hypoxia-inducible factor-2 involved in chemo/radioresistance in solid tumors. *Cancer Treat Rev.* 2015, 41, 623-33.

3) Löfstedt T.; Fredlund E.; Holmquist-Mengelbier L.; Pietras A.; Ovenberger M.; Poellinger L.; Påhlman S. Hypoxia inducible factor-2alpha in cancer. *Cell Cycle* 2007, 6, 919-26.

4) Nilsson, M.B.; Zage, P.E.; Zeng, L.; Xu, L.; Cascone, T.; Wu, H.K.; Saigal, B.; Zweidler-McKay, P.A.; Heymach, J.V. Multiple receptor tyrosine kinases regulate HIF-1alpha and HIF-2alpha in normoxia and hypoxia in neuroblastoma: implications for antiangiogenic mechanisms of multikinase inhibitors. *Oncogene* 2010, 20, 2938-49.

5) Cimmino, F.; Pezone, L.; Avitabile, M.; Acierno, G.; Andolfo, I.; Capasso, M.; Iolascon, A. Inhibition of hypoxia inducible factors combined with all-trans retinoic acid treatment enhances glial transdifferentiation of neuroblastoma cells. *Sci Rep.* 2015, DOI: 10.1038/srep11158.

6) De Miguel, M.P.; Alcaina, Y.; de la Maza, D.S.; Lopez-Iglesias, P. Cell metabolism under microenvironmental low oxygen tension levels in stemness, proliferation and pluripotency. *Curr Mol Med*. 2015, 15, 343-59.

7) Heddleston, J.M.; Li, Z.; McLendon, R.E.; Hjelmeland, A.B.; Rich, J.N. The hypoxic microenvironment maintains glioblastoma stem cells and promotes reprogramming towards a cancer stem cell phenotype. *Cell Cycle* 2009, 8**,** 3274-84.

8) Holmquist-Mengelbier, L.; Fredlund, E.; Lofstedt, T.; Noguera, R.; Navarro, S.; Nilsson, H.; Pietras, A.; Vallon-Christersson, J.; Borg, A.; Gradin, K.; Poellinger, L.; Påhlman, S. Recruitment of HIF-1alpha and HIF-2alpha to common targetgenes is differentially regulated in neuroblastoma: HIF-2alpha promotes an aggressive phenotype. *Cancer Cell* 2006, 10, 413–23.

9) Kim, W.Y.; Perera, S.; Zhou, B.; Carretero, J.; Yeh, J.J.; Heathcote, S.A.; Jackson, A.L.; Nikolinakos, P.; Ospina, B.; Naumov, G.; Brandstetter, K.A.; Weigman, V.J.; Zaghlul, S.; Hayes, D.N.; Padera, R.F.; Heymach, J.V.; Kung, A.L.; Sharpless, N.E.; Kaelin, W.G.; Wong, K.K. HIF2alpha cooperates with RAS to promote lung tumorigenesis in mice. *J Clin Invest* 2009, 119, 2160-70.

10) Burroughs, S.K.; Kaluz, S.; Wang, D.; Wang, K.; Van Meir, E.G.; Wang, B. Hypoxia inducible factor pathway inhibitors as anticancer therapeutics. *Future Med Chem* 2013, 5, 553-72.

11) Maris, J. M. Recent advances in neuroblastoma. *N Engl J Med* 2010, 362, 2202-11.

12) Mosse, Y.P.; Lim, M.S.; Voss, S.D.; Wilner, K.; Ruffner, K.; Laliberte, J.; Rolland, D.; Balis, F.M.; Maris, J.M.; Weigel, B.J.; Ingle, A.M.; Ahern, C.; Adamson, P.C.; Blaney, S.M. Safety and activity of crizotinib for paediatric patients with refractory solid tumours or anaplastic large-cell lymphoma: a Children's Oncology Group phase 1 consortium study. *Lancet Oncol* 2013, DOI: 10.1016/S1470-2045(13)70095-0.

13) Yu, A.L.; Gilman, A.L.; Ozkaynak, M.F.; London, W.B.; Kreissman, S.G.; Chen, H.X.; Smith, M.; Anderson, B.; Villablanca, J.G.; Matthay, K.K.; Shimada, H.; Grupp, S.A.;

Seeger, R.; Reynolds, C.P.; Buxton, A.; Reisfeld, R.A.; Gillies, S.D.; Cohn, S.L.; Maris, J.M.; Sondel, P.M.; Children's Oncology Group. Anti-GD2 antibody with GM-CSF, interleukin-2, and isotretinoin for neuroblastoma. *N Engl J Med* 2010, DOI: 10.1056/NEJMoa0911123.

14) Mohlin, S.; Hamidian, A.; Påhlman, S. HIF2A and IGF2 expression correlates in human neuroblastoma cells and normal immature sympathetic neuroblasts. *Neoplasia* 2013, 15, 328-34.

15) Cimmino, F.; Avitabile, M.; Pezone, L.; Scalia, G.; Montanaro, D.; Andreozzi, M.; Terracciano, L.; Iolascon, A.; Capasso, M. CD55 is a HIF-2α marker with anti-adhesive and pro-invading properties in neuroblastoma. *Oncogenesis*, 2016, DOI: 10.1038/oncsis.2016.20.

16) Cimmino, F.; Spano, D.; Capasso, M.; Zambrano, N.; Russo, R.; Zollo, M.; Iolascon, A. Comparative proteomic expression profile in all-trans retinoic acid differentiated neuroblastoma cell line. *J Proteome Res* 2007, 6, 2550-64.

17) Scippa, G.S.; Rocco, M.; Ialicicco, M.; Trupiano, D.; Viscosi, V.; Di Michele, M.; Arena, S.; Chiatante, D.; Scaloni, A. The proteome of lentil (*Lens culinaris* Medik.) seeds: discriminating between landraces. *Electrophoresis* 2010, 31, 497-506.

18) Buanne, P.; Renzone, G.; Monteleone, F.; Vitale, M.; Monti, S.M.; Sandomenico, A.; Garbi, C.; Montanaro, D.; Accardo, M.; Troncone, G.; Zatovicova, M.; Csaderova, L.; Supuran, C.T.; Pastorekova, S.; Scaloni, A.; De Simone, G.; Zambrano, N. Characterization of carbonic anhydrase IX interactome reveals proteins assisting its nuclear localization in hypoxic cells. *J Proteome Res.* 2013, 12, 282-92.

19) Persano, L.; Pistollato, F.; Rampazzo, E.; Della Puppa, A.; Abbadi, S.; Frasson, C.; Volpin, F.; Indraccolo, S.; Scienza, R.; Basso, G. BMP2 sensitizes glioblastoma stem-like cells to Temozolomide by affecting HIF-1α stability and MGMT expression. *Cell Death Dis*. 2012 DOI: 10.1038/cddis.2012.153.

20) Goeman, J.J.; van de Geer, S.A.; de Kort, F.; van Houwelingen, H.C. A global test for groups of genes: testing association with a clinical outcome. *Bioinformatics* 2004, 20, 93-99.

21) Schnekenburger, M.; Karius, T.; Diederich, M. Regulation of epigenetic traits of the glutathione S-transferase P1 gene: from detoxification toward cancer prevention and diagnosis. *Front Pharmacol*. 2014, DOI: 10.3389/fphar.2014.00170.

22) Mohlin, S.; Hamidian, A.; von Stedingk, K.; Bridges, E.; Wigerup, C.; Bexell, D.; Påhlman, S. PI3K-mTORC2 but not PI3K-mTORC1 regulates transcription of HIF2A/EPAS1 and vascularization in neuroblastoma. *Cancer Res.* 2015, 75, 4617-28.

23) Guo, X.; Chen, Q.R.; Song, Y.K.; Wei, J.S.; Khan, J. Exon array analysis reveals neuroblastoma tumors have distinct alternative splicing patterns according to stage and MYCN amplification status. *BMC Med Genomics* 2011, DOI: 10.1186/1755-8794-4-35.

24) Gao, R.; Yu, Y.; Inoue, A.; Widodo, N.; Kaul, S.C.; Wadhwa, R. Heterogeneous nuclear ribonucleoprotein K (hnRNP-K) promotes tumor metastasis by induction of genes involved in extracellular matrix, cell movement, and angiogenesis. *J Biol Chem.* 2013, 288, 15046-56.

25) Xu, Y.; Gao, X.D.; Lee, J.H.; Huang, H.; Tan, H.; Ahn, J.; Reinke, L.M.; Peter, M.E.; Feng, Y.; Gius, D.; Siziopikou, K.P.; Peng, J.; Xiao, X.; Cheng, C. Cell type-restricted activity of

hnRNPM promotes breast cancer metastasis via regulating alternative splicing. *Genes Dev.* 2014, 28, 1191-203.

26) Spraggon, L.; Dudnakova, T.; Slight, J.; Lustig-Yariv, O.; Cotterell, J.; Hastie, N.; Miles, C. hnRNP-U directly interacts with WT1 and modulates WT1 transcriptional activation. *Oncogene* 2007, 26, 1484-91.

27) Finka, A.; Sharma, S.K.; Goloubinoff, P. Multi-layered molecular mechanisms of polypeptide holding, unfolding and disaggregation by HSP70/HSP110 chaperones. *Front Mol Biosci.* 2015, DOI: 10.3389/fmolb.2015.00029.

28) Yang, H.; Xiong, Y.; Guan, K. Metabolic alteration in tumorigenesis. *Sci China Life Sci*. 2013, 56, 1067-75.

29) Chueh, F.Y.; Leong, K.F.; Cronk, R.J.; Venkitachalam, S.; Pabich, S.; Yu, C.L. Nuclear localization of pyruvate dehydrogenase complex-E2 (PDC-E2), a mitochondrial enzyme, and its role in signal transducer and activator of transcription 5 (STAT5)-dependent gene transcription. *Cell Signal.* 2011, 23, 1170-8.

30) Chen, R.; Xu, M.; Nagati, J.S.; Hogg, R.T.; Das, A.; Gerard, R.D.; Garcia, J.A. The acetate/ACSS2 switch regulates HIF-2 stress signaling in the tumor cell microenvironment. *PLoS One* 2015, DOI: 10.1371/journal.pone.0116515.

31) King, A.; Selak, M.A.; Gottlieb, E. Succinate dehydrogenase and fumarate hydratase: linking mitochondrial dysfunction and cancer. *Oncogene,* 2006, 25, 4675-82.

32) Cui, J.; Quan, M.; Jiang, W.; Hu, H.; Jiao, F.; Li, N.; Jin, Z.; Wang, L.; Wang, Y.; Wang, L. Suppressed expression of LDHB promotes pancreatic cancer progression via inducing glyco lytic phenotype. *Med Oncol.* 2015 DOI: 10.1007/s12032-015-0589-8.

33) Gautier, E.L.; Westerterp, M.; Bhagwat, N.; Cremers, S.; Shih, A.; Abdel-Wahab, O.; Lütjohann, D.; Randolph, G.J.; Levine, R.L.; Tall, A.R.; Yvan-Charvet, L. HDL and Glut1 inhibition reverse a hypermetabolic state in mouse models of myeloproliferative disorders. *J Exp Med.* 2013, 210, 339-53.

34) Kinlaw, W.B.; Baures, P.W.; Lupien, L.E.; Davis, W.L.; Kuemmerle, N.B. Fatty Acids and Breast Cancer: Make them on Site or have them Delivered. *J Cell Physiol.* 2016 DOI: 10.1002/jcp.25332.

35) Courtnay, R.; Ngo, D.C.; Malik, N.; Ververis, K.; Tortorella, S.M.; Karagiannis, T.C. Cancer metabolism and the Warburg effect: the role of HIF-1 and PI3K. *Mol Biol Rep.* 2015, 42, 841-51.

36) Sherwood, V. WNT signaling: an emerging mediator of cancer cell metabolism? *Mol Cell Biol*. 2015 DOI: 10.1128/MCB.00992-14.

37) Chesney, J.; Telang, S. Regulation of glycolytic and mitochondrial metabolism by ras. *Curr Pharm Biotechnol.* 2013, 14, 251-60.

38) Conrad, P.W.; Freeman, T.L.; Beitner-Johnson, D.; Millhorn, D.E. EPAS1 trans-activation during hypoxia requires p42/p44 MAPK. *J Biol Chem*. 1999, 274, 33709-13.

39) Eleveld, T.F.; Oldridge, D.A.; Bernard, V.; Koster, J.; Daage, L.C.; Diskin, S.J.; Schild, L.; Bentahar, N.B.; Bellini, A.; Chicard, M.; Lapouble, E.; Combaret, V.; Legoix-Né, P.; Michon, J.; Pugh, T.J.; Hart, L.S.; Rader, J.; Attiyeh, E.F.; Wei, J.S.; Zhang, S.; Naranjo, A.; Gastier-Foster, J.M.; Hogarty, M.D.; Asgharzadeh, S.; Smith, M.A.; Auvil, J.M.; Watkins, T.B.; Zwijnenburg, D.A.; Ebus, M.E.; van Sluis, P.; Hakkert, A.; van Wezel, E.; van der Schoot, C.E.; Westerhout, E.M.; Schulte, J.H.; Tytgat, G.A.; Dolman, M.E.; Janoueix-

Lerosey, I.; Gerhard, D.S.; Caron, H.N.; Delattre, O.; Khan, J.; Versteeg, R.; Schleiermacher, G.; Molenaar, J.J.; Maris, J.M. Relapsed neuroblastomas show frequent RAS-MAPK pathway mutations. *Nat Genet.* 2015, DOI: 10.1038/ng.3333.

40) Topisirovic, I.; Sonenberg, N. mRNA translation and energy metabolism in cancer: the role of the MAPK and mTORC1 pathways. *Cold Spring Harb Symp Quant Biol.* 2011, 76, 355-67.

41) Culjkovic, B.; Topisirovic, I.; Skrabanek, L.; Ruiz-Gutierrez, M.; Borden, K.L. eIF4E promotes nuclear export of cyclin D1 mRNAs via an element in the 3'UTR. *J Cell Biol.* 2005, 169, 245-56.

Figure Legends

Figure 1. Proteomic data obtained by comparing SHSY5Y-HIF-2α-overexpressing cells with respect to SHSY5Y-pcDNA counterparts. Western blotting was performed to test the cross-contamination of cytosolic (lane 1) and nuclear (lane 2) protein extracts from the SHSY5Y-HIF-2α cells (**A**). Isoelectric focusing on SHSY5Y-HIF-2α and SHSY5Y-pcDNA protein extracts was performed on immobilized pH gradient IPG gel strip, NL pH 3-11; proteins were further separated by 11% SDS-PAGE in the second dimension. Differentially represented spots that were picked-up on the preparative gel for further protein identification analysis are shown in the figure (**B**). Identified proteins were classified using the DAVID 2.1 beta annotation system. The Fisher exact test was used to determine the statistically significance of protein-enrichment in annotation terms. The functional categories and pathways are sorted by P-value (-log(P)). The category terms and the number of proteins are reported on Y-axis (**C**).

Figure 2. Validation of 2D-DIGE/nanoLC-ESI-LIT-MS/MS data. Western blot analysis of selected proteins was performed on the nuclear fraction from SHSY5Y-HIF-2α and SHSY5Y-pcDNA cells. H3 was used as the loading control (**A**). Protein bands were quantified by densitometry. The bar graph shows integral optic density (IOD) value for each band, normalized with respect to H3 expression (**B**). Oil red staining images of SHSY5Y-HIF-2α and SHSY5Y-pcDNA cells. The arrows indicate the lipid accumulation (**C**). Metabolic reactions altered by HIF-2α over-expression are sketched in (**D**).

Figure 3. RPPA data of HIF-2α-silenced and HIF-2α-over-expressing cells. Level plot showing *p*-values generated by the comparison of HIF-2α transgenic cell clones with their

relative controls for the expression/activation of 79 proteins, representative of JAK/STAT, NFKB, RAS/MAPK, SRC, WNT, AMPK, PI3K/AKT signalling pathways, apoptosis and cell cycle processes (**A**). Table showing pathway global test *p*-values obtained for RAS/MAPK, cell cycle, WNT and PI3K/AKT pathways for each considered comparison; $**p<0.05$, $*0.05<p<0.1$ (**B**). Level plot showing relative expression of proteins selected from global test analysis for each (RAS/MAPK, cell cycle, WNT and PI3K/AKT) significant pathway analyzed (**C**). Heat-map showing relative expression of proteins from selected pathways and clustering analysis (**D**). Western blot analysis of RB (S780), cyclin-E, Pan-RAS, p44/42 MAPK(Erk1/2) (T202/Y204), LEF1, AKT (S473), S6 Ribosomal Protein (S235/236), PDK1 (S241) proteins performed in SHSY5Y-shEPAS1 and SHSY5Y-HIF-2α cell clones and relative control cells. β-Actin expression has been used as loading control (**E**). Two clones (HIF-2α_A and HIF-2α_B) of SHSY5Y cells were engineered to over-express HIF-2α.

Figure 4. HIF-2α proteomic signature in NB patients. K-means clustering was used to subdivide gene expression data of freely available 498 primary NBs tumors of all stages (SEQC dataset) in two patients groups with high (POS) or low (NEG) activity of the HIF-2α proteome-gene set signature (**A**). Kaplan-Maier analysis for overall survival and relapse-free survival rates in patients with MYCN single copy (SEQC dataset) grouped for high (POS) or low (NEG) activity of the HIF-2α proteome-gene set signature (**B**).

Figure 1

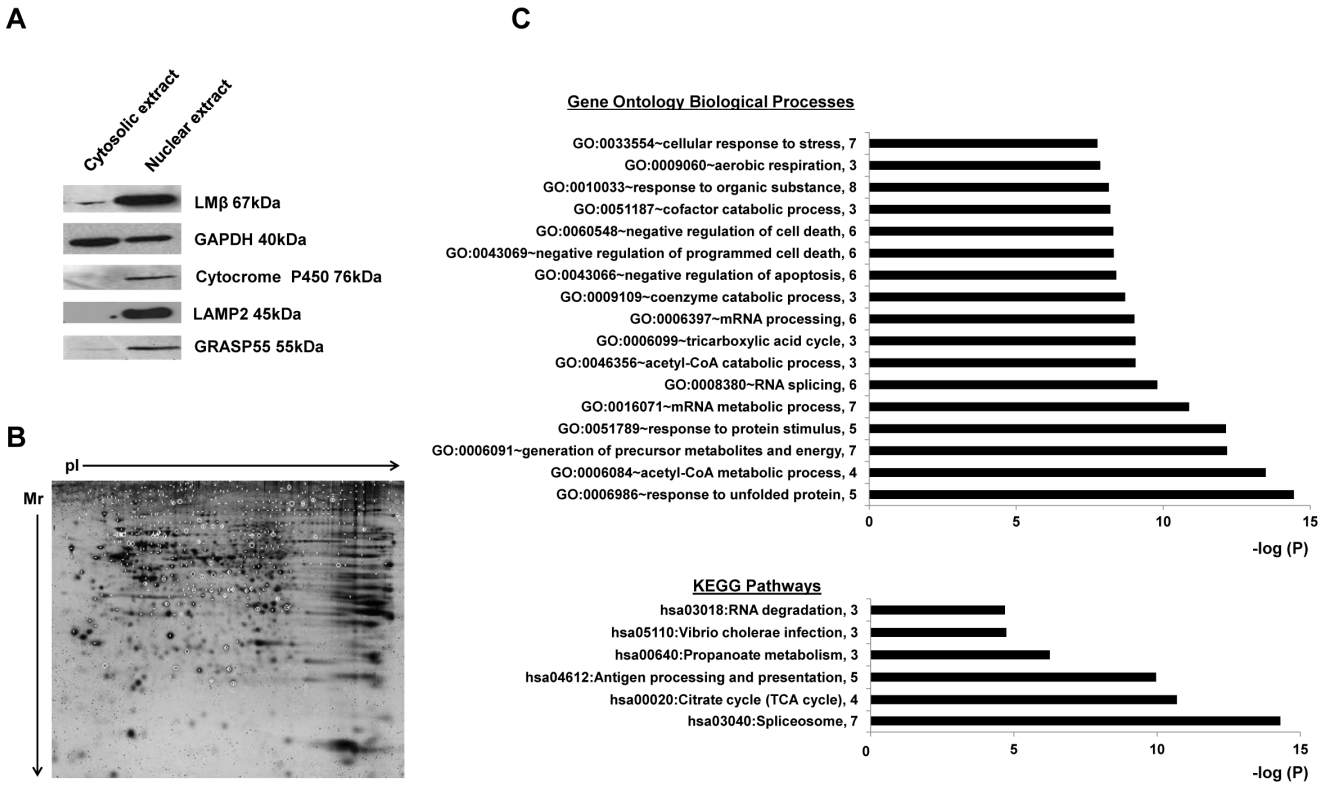
A
Cytosolic extract
Nuclear extract
LMβ 67kDa
GAPDH 40kDa
Cytocrome P450 76kDa
LAMP2 45kDa
GRASP55 55kDa
B
pI
Mr
C
Gene Ontology Biological Processes
GO:0033554~cellular response to stress, 7
GO:0009060~aerobic respiration, 3
GO:0010033~response to organic substance, 8
GO:0051187~cofactor catabolic process, 3
GO:0060548~negative regulation of cell death, 6
GO:0043069~negative regulation of programmed cell death, 6
GO:0043066~negative regulation of apoptosis, 6
GO:0009109~coenzyme catabolic process, 3
GO:0006397~mRNA processing, 6
GO:0006099~tricarboxylic acid cycle, 3
GO:0046356~acetyl-CoA catabolic process, 3
GO:0008380~RNA splicing, 6
GO:0016071~mRNA metabolic process, 7
GO:0051789~response to protein stimulus, 5
GO:0006091~generation of precursor metabolites and energy, 7
GO:0006084~acetyl-CoA metabolic process, 4
GO:0006986~response to unfolded protein, 5
0
5
10
15
-log (P)
KEGG Pathways
hsa03018:RNA degradation, 3
hsa05110:Vibrio cholerae infection, 3
hsa00640:Propanoate metabolism, 3
hsa04612:Antigen processing and presentation, 5
hsa00020:Citrate cycle (TCA cycle), 4
hsa03040:Spliceosome, 7
0
5
10
15
-log (P)

Figure 2

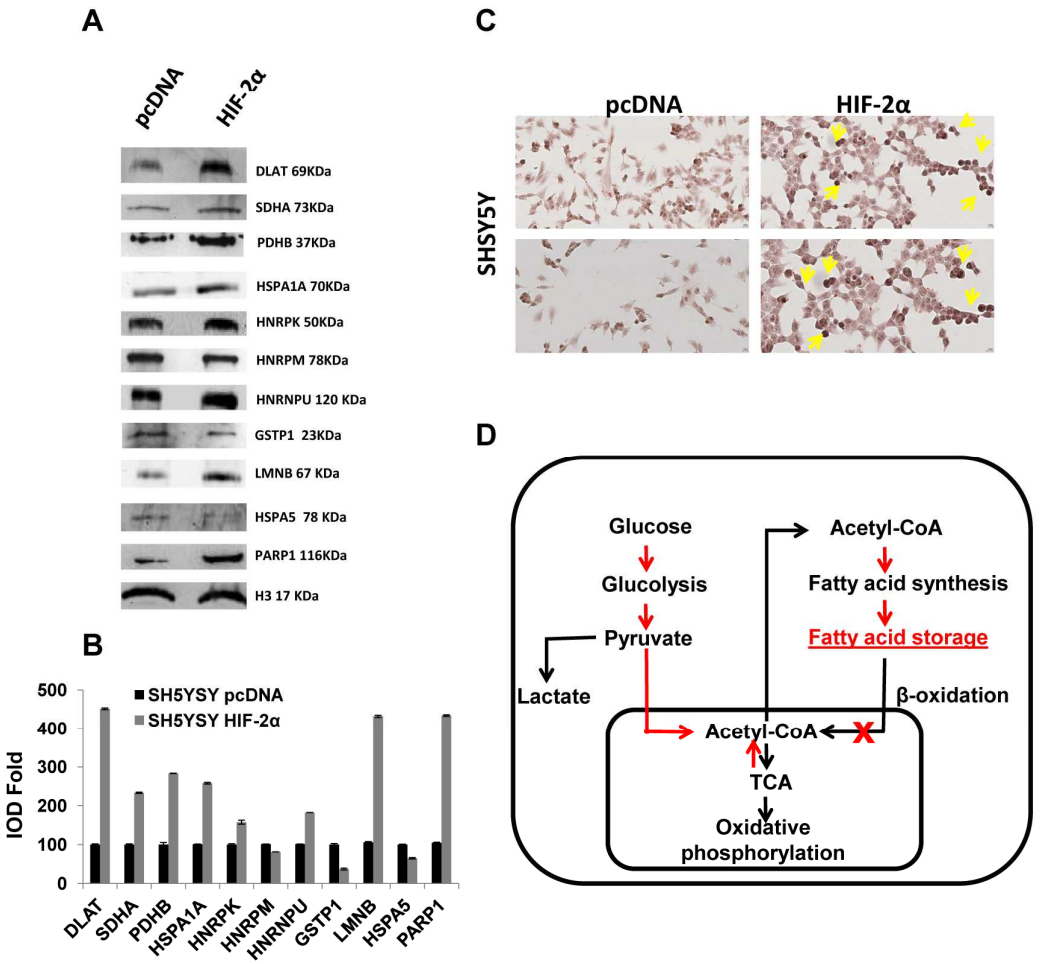
A
pcDNA
HIF-2α
DLAT 69KDa
SDHA 73KDa
PDHB 37KDa
HSPA1A 70KDa
HNRPK 50KDa
HNRPM 78KDa
HNRNPU 120 KDa
GSTP1 23KDa
LMNB 67 KDa
HSPA5 78 KDa
PARP1 116KDa
H3 17 KDa
B
SH5YSY pcDNA
SH5YSY HIF-2α
IOD Fold
500
400
300
200
100
0
DLAT
SDHA
PDHB
HSPA1A
HNRPK
HNRPM
HNRNPU
GSTP1
LMNB
HSPA5
PARP1
C
pcDNA
HIF-2α
SHSY5Y
D
Glucose
Glucolysis
Pyruvate
Lactate
Acetyl-CoA
Fatty acid synthesis
Fatty acid storage
β-oxidation
Acetyl-CoA
TCA
Oxidative
phosphorylation

Figure 3

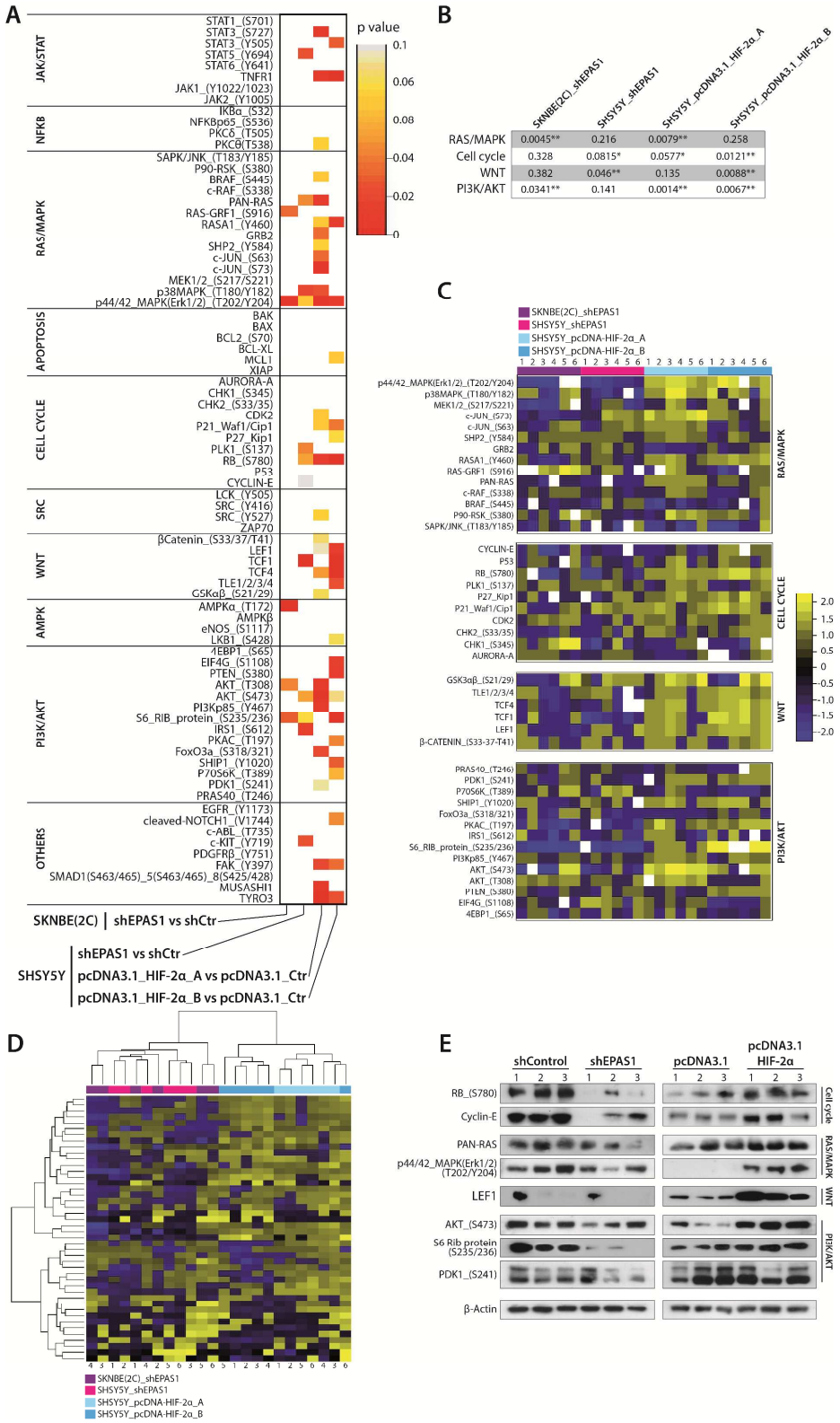
A
JAK/STAT
STAT1_(S701)
STAT3_(S727)
STAT3_(Y505)
STAT5_(Y694)
STAT6_(Y641)
TNFR1
JAK1_(Y1022/1023)
JAK2_(Y1005)
NFKB
IKBα_(S32)
NFKBp65_(S536)
PKCδ_(T505)
PKCθ(T538)
RAS/MAPK
SAPK/JNK_(T183/Y185)
P90-RSK_(S380)
BRAF_(S445)
c-RAF_(S338)
PAN-RAS
RAS-GRF1_(S916)
RASA1_(Y460)
GRB2
SHP2_(Y584)
c-JUN_(S63)
c-JUN_(S73)
MEK1/2_(S217/S221)
p38MAPK_(T180/Y182)
p44/42_MAPK(Erk1/2)_(T202/Y204)
APOPTOSIS
BAK
BAX
BCL2_(S70)
BCL-XL
MCL1
XIAP
CELL CYCLE
AURORA-A
CHK1_(S345)
CHK2_(S33/35)
CDK2
P21_Waf1/Cip1
P27_Kip1
PLK1_(S137)
RB_(S780)
P53
CYCLIN-E
SRC
LCK_(Y505)
SRC_(Y416)
SRC_(Y527)
ZAP70
WNT
βCatenin_(S33/37/T41)
LEF1
TCF1
TCF4
TLE1/2/3/4
GSKαβ_(S21/29)
AMPK
AMPKα_(T172)
AMPKβ
eNOS_(S1117)
LKB1_(S428)
PI3K/AKT
4EBP1_(S65)
EIF4G_(S1108)
PTEN_(S380)
AKT_(T308)
AKT_(S473)
PI3Kp85_(Y467)
S6_RIB_protein_(S235/236)
IRS1_(S612)
PKAC_(T197)
FoxO3a_(S318/321)
SHIP1_(Y1020)
P70S6K_(T389)
PDK1_(S241)
PRAS40_(T246)
OTHERS
EGFR_(Y1173)
cleaved-NOTCH1_(V1744)
c-ABL_(T735)
c-KIT_(Y719)
PDGFRβ_(Y751)
FAK_(Y397)
SMAD1(S463/465)_5(S463/465)_8(S425/428)
MUSASHI1
TYRO3
p value
0.1
0.06
0.08
0.04
0.02
0
SKNBE(2C) | shEPAS1 vs shCtr
SHSY5Y
shEPAS1 vs shCtr
pcDNA3.1_HIF-2α_A vs pcDNA3.1_Ctr
pcDNA3.1_HIF-2α_B vs pcDNA3.1_Ctr
B
SKNBE(2C)_shEPAS1
SHSY5Y_shEPAS1
SHSY5Y_pcDNA3.1_HIF-2α_A
SHSY5Y_pcDNA3.1_HIF-2α_B
RAS/MAPK 0.0045** 0.216 0.0079** 0.258
Cell cycle 0.328 0.0815* 0.0577* 0.0121**
WNT 0.382 0.046** 0.135 0.0088**
PI3K/AKT 0.0341** 0.141 0.0014** 0.0067**
C
SKNBE(2C)_shEPAS1
SHSY5Y_shEPAS1
SHSY5Y_pcDNA-HIF-2α_A
SHSY5Y_pcDNA-HIF-2α_B
1 2 3 4 5 6 1 2 3 4 5 6 1 2 3 4 5 6
p44/42_MAPK(Erk1/2)_(T202/Y204)
p38MAPK_(T180/Y182)
MEK1/2_(S217/S221)
c-JUN_(S73)
c-JUN_(S63)
SHP2_(Y584)
GRB2
RASA1_(Y460)
RAS-GRF1_(S916)
PAN-RAS
c-RAF_(S338)
BRAF_(S445)
P90-RSK_(S380)
SAPK/JNK_(T183/Y185)
RAS/MAPK
CYCLIN-E
P53
RB_(S780)
PLK1_(S137)
P27_Kip1
P21_Waf1/Cip1
CDK2
CHK2_(S33/35)
CHK1_(S345)
AURORA-A
CELL CYCLE
GSK3αβ_(S21/29)
TLE1/2/3/4
TCF4
TCF1
LEF1
β-CATENIN_(S33-37-T41)
WNT
PRAS40_(T246)
PDK1_(S241)
P70S6K_(T389)
SHIP1_(Y1020)
FoxO3a_(S318/321)
PKAC_(T197)
IRS1_(S612)
S6_RIB_protein_(S235/236)
PI3Kp85_(Y467)
AKT_(S473)
AKT_(T308)
PTEN_(S380)
EIF4G_(S1108)
4EBP1_(S65)
PI3K/AKT
2.0
1.5
1.0
0.5
0
-0.5
-1.0
-1.5
-2.0
D
SKNBE(2C)_shEPAS1
SHSY5Y_shEPAS1
SHSY5Y_pcDNA-HIF-2α_A
SHSY5Y_pcDNA-HIF-2α_B
E
shControl
shEPAS1
pcDNA3.1
pcDNA3.1 HIF-2α
1 2 3 1 2 3 1 2 3 1 2 3
RB_(S780)
Cyclin-E
PAN-RAS
p44/42_MAPK(Erk1/2) (T202/Y204)
LEF1
AKT_(S473)
S6 Rib protein (S235/236)
PDK1_(S241)
β-Actin
Cell cycle
RAS/MAPK
WNT
PI3K/AKT

Figure 4

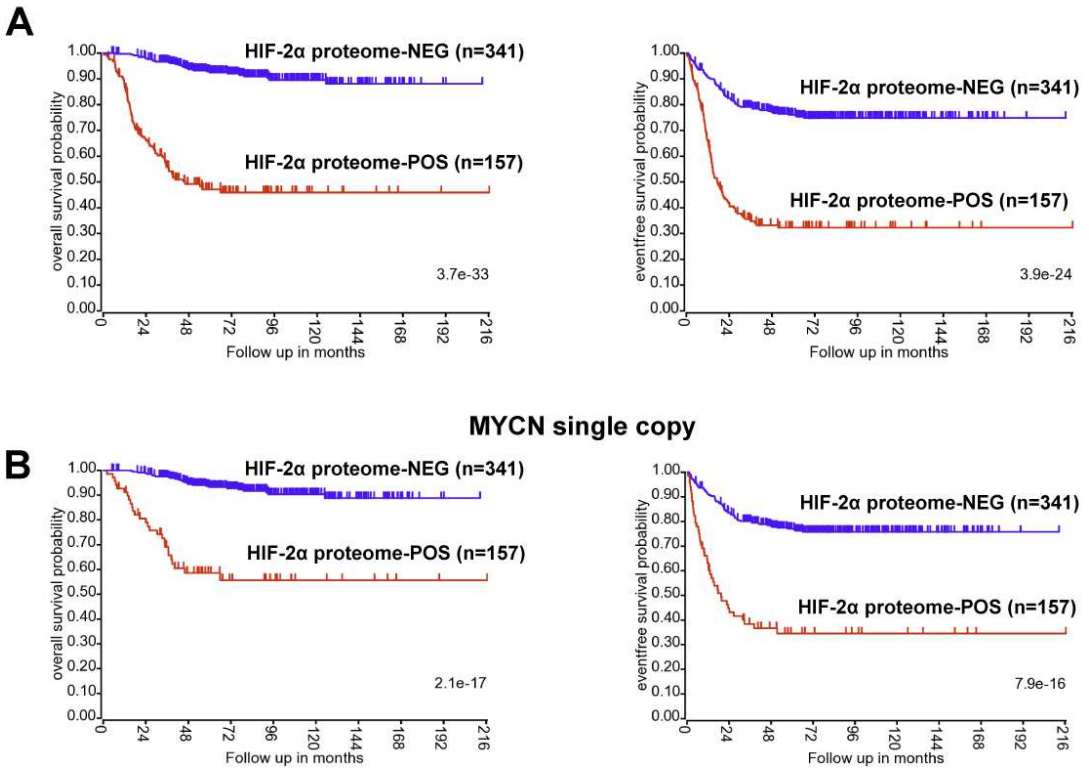
A
HIF-2α proteome-NEG (n=341)
HIF-2α proteome-POS (n=157)
overall survival probability
3.7e-33
Follow up in months
HIF-2α proteome-NEG (n=341)
HIF-2α proteome-POS (n=157)
eventfree survival probability
3.9e-24
Follow up in months
MYCN single copy
B
HIF-2α proteome-NEG (n=341)
HIF-2α proteome-POS (n=157)
overall survival probability
2.1e-17
Follow up in months
HIF-2α proteome-NEG (n=341)
HIF-2α proteome-POS (n=157)
eventfree survival probability
7.9e-16
Follow up in months

Table 1. Proteins showing quantitative changes in the SHSY5Y-HIF-2α-over-expressing vs SHSY5Y-pcDNA cell comparison, as deduced by 2D-DIGE and identified by nanoLC-ESI-LIT-MS/MS. Spot number, NCBI accession, protein name, Mascot score, number of assigned and assigned unique peptides, sequence coverage (%), relative fold change and gene symbol are listed. Fold change was ascertained as reported in the experimental section. N.a., not available.

Spot	NCBI Code	Description	Identification score	Peptides	Unique peptides	Sequence coverage (%)	Fold 2D-DIGE	Gene Symbol
214	gi|62022572|gb|AAH50564.1|	SWI/SNF related, matrix associated, actin-dependent regulator of chromatin	229	6	6	5.6	-1.25	SMARCC1
398	gi|3202000|gb|AAC19382.1|	Scaffold attachment factor A	457	12	10	10.9	2.23	HNRNPU
401	gi|119569943|gb|EAW49558.1|	Chondroitin sulfate proteoglycan 6 (bamacan), isoform CRA_b	484	10	10	10.8	2.36	SMC3
417	gi|999380|gb|AAB34405.1|	Mitosis-specific chromosome segregation protein SMC1 homolog	272	5	5	4.9	4.12	SMC1A
485	gi|23342633|emb|CAD48681.1|	Neurolysin, mitochondrial	227	5	5	9.9	-8.18	n.a.
503	gi|516764|dbj|BAA04654.1|	Motor protein	254	5	5	9.4	-17.69	HMP
510	gi|292059|gb|AAA67526.1|	MTHSP75	849	16	15	30.8	-10.75	HSPA9
	gi|16306859|gb|AAH06551.1|	Lamin B2	372	7	7	13.8		LMNB2
529	gi|347134|gb|AAA20683.1|	Succinate dehydrogenase flavoprotein subunit	471	10	9	14.2	2.01	SDHA
	gi|34228|emb|CAA27173.1|	Lamin isoform A-delta50	383	8	8	14.7		LMNA
552	gi|292059|gb|AAA67526.1|	MTHSP75	1551	31	26	48.2	1.89	HSPA9
	gi|32467|emb|CAA68445.1|	71 kDa heat shock cognate protein	474	10	10	19.3		HSPA8
	gi|16306859|gb|AAH06551.1|	Lamin B2	435	8	8	15.7		LMNB2
	gi|119530|sp|P13667.2|PDIA4_HUMAN	Protein disulfide-isomerase A4	323	6	6	12.6		PDIA4
556	gi|292059|gb|AAA67526.1|	MTHSP75	1250	27	23	44.3	2.25	HSPA9
	gi|32467|emb|CAA68445.1|	71 kDa heat shock cognate protein	1147	27	23	41.2		HSPA8
	gi|16306859|gb|AAH06551.1|	Lamin B2	478	9	9	15.5		LMNB2
	gi|119530|sp|P13667.2|PDIA4_HUMAN	Protein disulfide-isomerase A4	422	9	9	17.2		PDIA4
	gi|188492|gb|AAA63228.1|	Heat shock-induced protein	329	7	7	15.1		HSPA1L
577	gi|62087562|dbj|BAD92228.1|	Succinate dehydrogenase complex, subunit A, flavoprotein precursor variant	588	12	10	22.1	3.01	SDHA
583	gi|347134|gb|AAA20683.1|	Succinate dehydrogenase flavoprotein subunit	807	16	16	30.7	3.38	SDHA
594	gi|130781|sp|P09874.4|PARP1_HUMAN	Poly [ADP-ribose] polymerase 1	279	5	5	6.8	3.09	PARP1
603	gi|6470150|gb|AAF13605.1|AF188611_1	BiP protein	315	6	6	13.3	-8.02	HSPA5

604	gi|6470150|gb|AAF13605.1|AF188611_1	BiP protein	418	8	8	15.5	-13.2	HSPA5
	gi|114549|sp|P06576.3|ATPB_HUMAN	ATP synthase subunit beta, mitochondrial	361	7	7	16.6		ATP5B
605	gi|32467|emb|CAA68445.1|	71 kDa heat shock cognate protein	1317	36	26	44.1	2.18	HSPA8
	gi|16306859|gb|AAH06551.1|	Lamin B2	1214	25	22	35		LMNB2
	gi|15341906|gb|AAH13138.1|	ATPase, H^+ transporting, lysosomal 70kDa, V1 subunit A	454	11	10	23.5		ATP6V1A
	gi|188488|gb|AAA63226.1|	Heat shock-induced protein	451	8	8	15.8		HSPA1A
	gi|189053456|dbj|BAG35622.1|	Heat shock 70 kDa protein 6	243	6	5	11.4		HSPA6
608	gi|6470150|gb|AAF13605.1|AF188611_1	BiP protein	214	6	5	10.8	-12.43	HSPA5
609	gi|16306859|gb|AAH06551.1|	Lamin B2	1478	43	30	44.5	2.77	LMNB2
	gi|188488|gb|AAA63226.1|	Heat shock-induced protein	612	17	13	23.4		HSPA1A
610	gi|4529893|gb|AAD21816.1|	HSP70-1	1195	44	25	39.2	3.39	HSPA1A
	gi|194388088|dbj|BAG65428.1|	Heat shock 70 kDa protein 1A/1B	1147	43	24	40.4		HSPA1A
	gi|16306859|gb|AAH06551.1|	Lamin B2	476	10	10	18.7		LMNB2
	gi|35360|emb|CAA68787.1|	PDC-E2 precursor	387	9	8	15.4		DLAT
663	gi|135538|sp|P17987.1|TCPA_HUMAN	T-complex protein 1 subunit alpha	466	8	8	17.1	2.64	TCP1
668	gi|38458|emb|CAA50283.1|	PTB-associated splicing factor	304	7	7	11.7	-1.36	SFPQ
671	gi|37545|emb|CAA45409.1|	Splicing factor U2AF	196	6	4	14.5	1.74	U2AF2
689	gi|129379|sp|P10809.2|CH60_HUMAN	60 kDa heat shock protein, mitochondrial	705	13	12	28.3	2.85	HSPD1
	gi|241478|gb|AAB20770.1|	Heterogeneous nuclear ribonucleoprotein complex K	390	9	8	23.1		HNRNPK
	gi|37850|emb|CAA39600.1|	Vimentin	347	7	7	18.5		VIM
699	gi|129379|sp|P10809.2|CH60_HUMAN	60 kDa heat shock protein, mitochondrial	1004	23	18	40.8	2.33	HSPD1
	gi|241478|gb|AAB20770.1|	Heterogeneous nuclear ribonucleoprotein complex K	525	14	10	24.8		HNRNPK
840	gi|6841066|gb|AAF28888.1|AF123303_1	Calcium-binding transporter	235	5	4	12.7	-4.01	SLC25A24
895	gi|33150622|gb|AAP97189.1|AF087890_1	Beta-succinyl CoA synthetase	592	15	12	36.5	3.6	SUCLA2
898	gi|901998|gb|AAA70033.1|	TAR DNA-binding protein-43	341	7	7	21.3	-8.03	TARDBP
906	gi|34138|emb|CAA68809.1|	Ornithine aminotransferase, mitochondrial isoform 1 precursor	413	9	8	23.7	-5.88	OAT
	gi|45710075|gb|AAH14519.1|	Solute carrier family 25 (mitochondrial carrier; phosphate carrier), member 24	488	9	7	23.3		SLC25A24
	gi|15679945|gb|AAH14279.1|	Vesicle amine transport protein 1 homolog (*T. californica*)	353	7	6	21.9		VAT1
913	gi|49457530|emb|CAG47064.1|	CKB	576	14	9	30.7	-11.61	CKB
	gi|28252|emb|CAA25099.1|	Actin, cytoplasmic 1	243	8	5	18.9		ACTB
976	gi|12803583|gb|AAH02625.1|	Heterogeneous nuclear ribonucleoprotein A/B	398	8	8	28.1	-3.07	HNRNPAB
998	gi|12803583|gb|AAH02625.1|	Heterogeneous nuclear ribonucleoprotein A/B	496	11	9	25.3	-3.34	HNRNPAB
1011	gi|28422556|gb|AAH47024.1|	Succinate-CoA ligase, GDP-forming, beta subunit	624	17	14	38.8	-7.55	SUCLG2

	gi|6456118|gb|AAF09142.1|AF190167_1	Membrane-associated protein SLP-2	555	10	10	38.8		STOML2
	gi|546088|gb|AAB30320.1|	Cytoplasmic antiproteinase	288	5	5	19.9		n.a.
1013	gi|34329|emb|CAA68701.1|	L-lactate dehydrogenase B chain	209	5	5	19	-15.53	LDHB
1021	gi|62089046|dbj|BAD92970.1|	Heterogeneous nuclear ribonucleoprotein M isoform a variant	285	5	5	9.9	-2.89	HNRNPM
1066	gi|194390304|dbj|BAG61914.1|	Heterogeneous nuclear ribonucleoprotein D-like isoform a	340	7	7	30.3	-3.58	HNRNPDL
	gi|762885|gb|AAA64895.1|	Plakoglobin	256	6	6	9.8		JUP
1083	gi|119339|sp|P06733.2|ENOA_HUMAN	Alpha-enolase	850	16	13	41.5	-2.72	ENO1
1088	gi|12803583|gb|AAH02625.1|	Heterogeneous nuclear ribonucleoprotein A/B	277	5	5	24.2	-25.68	HNRNPAB
1091	gi|35451|emb|CAA50197.1|	Serine/threonine specific protein phosphatase	210	5	5	18.5	-2.7	n.a.
1092	gi|9836652|dbj|BAB11885.1|	BSCv	326	7	6	18.2	-20.95	APMAP
	gi|131467|sp|P18031.1|PTN1_HUMAN	Tyrosine-protein phosphatase non-receptor type 1	267	5	5	14.5		PTPN1
1093	gi|5542020|gb|AAD45179.1|L32610_1	Ribonucleoprotein	266	5	5	19.1	-18.1	n.a.
1217	gi|682748|dbj|BAA08389.1|	Antioxidant protein 1	356	11	8	28.5	3.97	PRDX3
1220	gi|799381|gb|AAB95175.1|	Antioxidant enzyme AOE37-2	369	8	7	32.1	3.77	PRDX4
1289	gi|1922287|emb|CAA66808.1|	Enoyl-CoA hydratase	683	16	11	39.3	-7.88	ECHS1
1387	gi|2076717|gb|AAC51280.1|	Glutathione S-transferase	490	11	8	52.4	-3.07	GSTP1

“for TOC only”

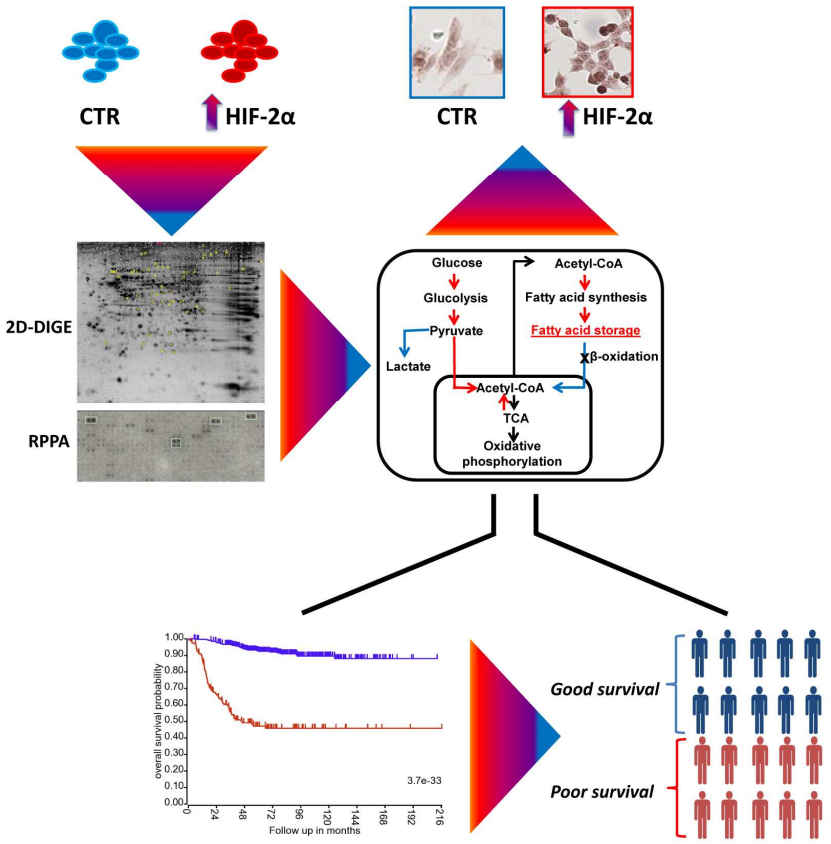
CTR
HIF-2α
CTR
HIF-2α
2D-DIGE
RPPA
Glucose
Glucolysis
Pyruvate
Lactate
Acetyl-CoA
Fatty acid synthesis
Fatty acid storage
β-oxidation
Acetyl-CoA
TCA
Oxidative phosphorylation
overall survival probability
3.7e-33
Follow up in months
Good survival
Poor survival